Graphical Abstract

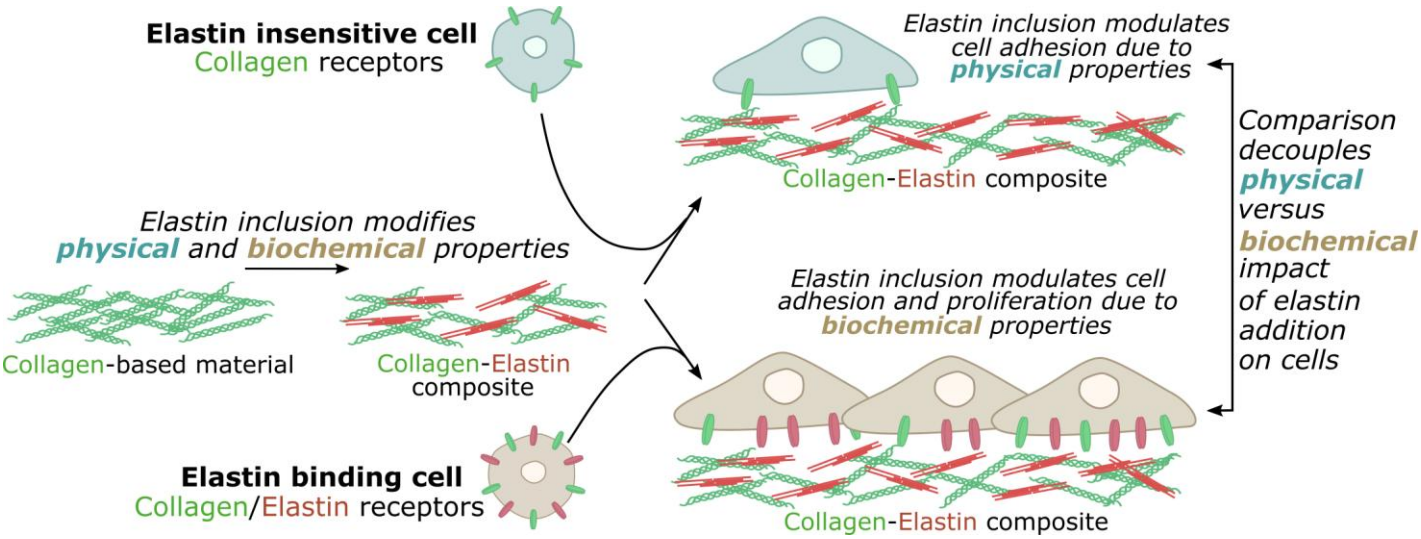

Cellular response to collagen-elastin composite materials

Daniel V. Bax[1,2#*], Helen E. Smalley[1#], Richard W. Farndale[2], Serena M. Best[1], Ruth E. Cameron[1]

[1] Department of Materials Science and Metallurgy, University of Cambridge, 27 Charles Babbage Road, Cambridge, CB3 0FS, United Kingdom

[2] Department of Biochemistry, University of Cambridge, Downing Site, Cambridge, CB2 1QW, United Kingdom

[#] These authors contributed equally

*Corresponding author Tel.: +44 1223 334560; fax: +44 1223 334567.

E-mail address: dvb24@cam.ac.uk

Keywords: collagen, elastin, cellular response

1. Abstract

Collagen is used extensively in tissue engineering due to its biocompatibility, near-universal tissue distribution, low cost and purity. However, native tissues are composites that include diverse extracellular matrix components, which influence strongly their mechanical and biological properties. Here, we provide important new findings on the differential regulation, by collagen and elastin, of the bio-response to the composite material. Soluble and insoluble elastin had differing effects on the stiffness and failure strength of the composite films. We established that Rugli cells bind elastin via EDTA-sensitive receptors, whilst HT1080 cells do not. These cells allowed us to probe the contribution of collagen alone (HT1080) and collagen plus elastin (Rugli) to the cellular response. In the presence of elastin, Rugli cell attachment, spreading and proliferation increased, presumably through elastin-binding receptors. By comparison, the attachment and spreading of HT1080 cells was modified by elastin inclusion, but without affecting their proliferation, indicating indirect modulation by elastin of the response of cells to collagen. These new insights highlight that access to elastin dominates the cellular response when elastin-binding receptors are present. In the absence of these receptors, modification of the collagen component and/or physical properties dictate the cellular response. Therefore, we can attribute the contribution of each constituent on the ultimate bioactivity of heterogeneous collagen-composite materials, permitting informed, systematic biomaterials design.

2. Introduction

Purified extracellular matrix (ECM) components are often utilised for scaffold fabrication in tissue engineering applications as they provide both physical and biochemical cues to guide tissue development [1]. As such they can recreate the cellular environment of native tissue. The ECM of tissue is comprised of a complex organisation of macromolecules such as collagen, laminin and elastin, and glycosaminoglycans (GAGs). Fibrillar collagen type I is the most abundant of these ECM proteins comprising ~30% of the total protein mass in humans [2], where it provides strength, stiffness and cell ligating motifs. Additionally isolated collagen possesses appropriate biocompatiblility, biodegradability, purity and cost which makes it an ideal candidate as a scaffold precursor material [1].

Chemical or physical crosslinkers are frequently used to enhance the physical integrity of collagen-based biomaterials. Of these, the most commonly used employs 1-ethyl-3-(3-dimethylaminopropyl)-carbodiimide hydrochloride (EDC) in the presence of N-hydroxysuccinimide (NHS), as any cytotoxic reagents and products are simply removed by washing [3]. This allows discrete control over the mechanical properties and degradation kinetics of the collagen-based material [3–5]. Evaluation of thermal shrinkage and primary amine content has led to the commonly used ratio of 5 EDC : 2 NHS : 1 COOH group on collagen in a 75% ethanol solution for 2-4 hours as an optimal condition. We have chosen to use this ratio here as it yields a maximal crosslinking density [4,6–8]. EDC cross-links proteins through carboxylic acid groups on aspartic and glutamic acid residues and neighbouring primary amine groups, however this can be detrimental to cell interaction [9]. In particular native-like cell adhesion through cell-surface heterodimeric, transmembrane integrins is lost, which is replaced with non-native interactions that do not support cell proliferation [9]. Of the 24 different integrin pairs [10], collagen associates with integrins $\alpha_1\beta_1$, $\alpha_2\beta_1$, $\alpha_{10}\beta_1$,and $\alpha_{11}\beta_1$, via an inserted A domain (I domain) within the α subunit of the

integrin [11,12]. These I domains bind to the consensus Gxx′GEx″ (single amino acid code) sequences in collagen [13–16]. The critical dependence on the carboxylic group contained on the glutamic acid (E) residue [17] of this sequence gives the intriguing hypothesis that chemical crosslinking of collagen competes with integrin adhesion for the same chemical groups [9,18], necessitating refunctionalisation of collagen films after cross-linking [19].

Despite the recent interest in collagen-based materials, it is ambiguous whether collagen-only materials adequately recapitulate the complex mechanical and biochemical properties of native tissue. Therefore, inclusion of additional ECM components, such as elastin, offers the opportunity to tailor the bio-response to the composite material. Elastin represents an attractive additive as it is provides elastic recoil of a range of tissues [20] and interacts with cells via a number of cell surface receptors. These include the elastin-binding protein (EBP) [21,22], cell surface heparan and chondroitin sulphate-containing glycosaminoglycans (GAGs) [23] and cell surface integrins $\alpha_V\beta_3$ and $\alpha_V\beta_5$ [24–26]. As such, elastin has been examined for biomaterials fabrication. To date a variety of elastin precursors have been employed, including native elastin, insoluble elastin (IE), soluble elastin (SE), tropoelastin and synthetic elastin-like polypeptides (ELPs) [27]. When fabricated solely from purified elastin, for example through electrospinning [28], or by decellularising natural tissues [29], elastin-based materials interact with a range of cell types exhibit non-thrombogenic potential and are remodelled *in vivo* [30]. As for materials fabricated solely from collagen, these elastin-only materials do not fully replicate the complex mechanics and biochemical attributes of tissues. Therefore, elastin has been incorporated into composites containing other ECM proteins, in particular collagen I, which offer huge potential as they possess complex mechanical properties that are similar to native tissue. For example inclusion of elastin into collagen-based materials reduces the specific tensile and compressive moduli [31]. To further recreate the fibrillar tissue architecture, elastin and collagen have

been simultaneously electrospun to produce co-deposited fibrous materials [32], however, to reduce complexity, here we have explored amorphous materials of insoluble collagen and elastin.

Although the physical properties of collagen-elastin composite materials are well established [31], there is conflicting biochemical data showing both an increased and decreased cell proliferation upon elastin addition. This discrepancy is presumably due to the different assay parameters utilised for each study [33]. For example short term studies on fibroblasts and myoblasts showed little effect of IE addition to collagen [7,18] whilst others have observed decreased cell proliferation [34,35]. Similarly vascular smooth muscle cell proliferation has been inhibited [31] or promoted [36] with IE addition, although the overall consensus is that addition of elastin reduces SMC proliferation [37]. Likewise, SE has been shown to increase fibroblast proliferation [38] whilst others observe selective stimulation of keratinocyte but not fibroblast proliferation [39]. We hypothesise that this wide range of responses is due to cell-type specific ligation with the collagen and elastin components of these composites. In particular, we note that the relative contribution of the collagen and elastin components to the cellular response, and the timescale over which these effects occur, is unclear. Therefore, the aim of this study was to understand the cell-biological response to the collagen and elastin components in IE- and SE-collagen composite materials. To undertake this analysis we utilised two different model cell lines, rat glioma cells (Ruglis) and human fibrosarcoma cells (HT1080s), which exhibited differential binding properties to elastin, allowing us to delineate the cellular behaviour in the presence and absence of elastin ligation by the cell. This has enabled us to probe the specific bio-activity of collagen-elastin composites over biologically important time frames, illustrating the importance of the elastin-engagement in this response.

3. Materials and Methods

3.1. Materials

Unless stated otherwise all reagents were purchased from Sigma Aldrich UK. 4 % v/v acetic acid was purchased from Alfa Aesar. Silicone moulds for producing films were purchased from Lakeland Ltd. (Windermere, UK).

3.2. Amino acid analysis

Approximately 1mg samples were subjected to amino acid analysis (Department of Biochemistry, University of Cambridge, UK). The percentage content of each amino acid was determined by correcting against a norleucine standard and then dividing the measured µmole of each amino acid/mg of sample by the total µmole of all measured amino acids. Cystine and tryptophan were not measured, however they are absent from collagen and represent trace amino acids in elastin. The predicted amino acid content was derived from the primary amino acid sequence of bovine elastin (UniProtKB-P04985), bovine collagen alpha I (I) (UniProtKB-P02453) and bovine collagen alpha 2 (I) (UniProtKB-P02465).

3.3. Slurry preparation

1 wt% suspensions of bovine insoluble Achilles tendon collagen, insoluble bovine neck ligament elastin (IE) and soluble bovine neck ligament elastin (E6527 [40] - SE) were swollen in 0.05 M acetic acid overnight at 4 °C. These were homogenised in a beaker on ice using a VWR VDI25 homogeniser for 5 min at 6500 rpm followed by 25 min at 13500 rpm for collagen, for 5 min at 6500 rpm followed by 10 min at 13500 rpm for IE, and for 5 min at 6500 rpm followed by 5 min at 13500 rpm for SE. Mixed compositions were obtained by manually mixing appropriate volumes of the 1 wt% stock suspensions. All of the protein

suspensions had a final concentration of 1 wt%. Suspensions that did not contain IE were degassed by centrifuging for 5 min at 3250 g (2500 rpm) in a Hermle Z300 centrifuge. Suspensions containing IE were degassed for 2 min at 14 mTorr in a VirTis advantage freeze-dryer to prevent sedimentation of the IE component. We define SE alone as a solution and SE in combination with insoluble collagen as a suspension.

3.4. Film preparation

Films for SEM and mechanical testing were cast in 40 mm diameter circular silicone moulds. 1 mL of suspension was added to each mould, and any bubbles were removed. Films for cell adhesion and proliferation analysis were prepared by casting 400 μL or 200 μL of slurry into wells of 24- and 48-well plates respectively. Films for cell imaging were cast by applying 50 μL protein slurry onto the centre of 13 mm diameter glass coverslips, placed in a 24 well plate. All samples were dried in a fume hood for 2 days. Films were crosslinked using a solution containing a molar ratio of 5 EDC : 2 NHS in 70 % ethanol with a final EDC concentration of 12 mM. 800 μL, 400 μL or 5 ml of crosslinking solution was added to each sample in 24-well plates, 48-well plates or 40 mm silicone moulds respectively. The samples were covered and incubated at room temperature on a rocker at 50 rpm for 2 h. Once cross-linking was completed the samples were washed for 5 x 5 min in H_2O whilst rocking at 50 rpm. They were then dried in a fume hood for 48 h.

3.5. Enzyme-linked Immunosorbent Analysis (ELISA)

Films were washed with 3 x 1 mL aliquots of PBS then blocked with 2 % (w/v) bovine serum albumin (BSA) in wash buffer (0.1 %(v/v) Tween-20, 1 mg/mL BSA in PBS) for 1 h at room temperature. The samples were washed with 3 x 1 mL wash buffer and then incubated in 0.75 mL of 1:2000 diluted mouse anti-elastin antibody (clone BA-4) in wash

buffer for 1 h at room temperature. The antibody was aspirated, and the samples were washed in 3 x 1 mL wash buffer before incubation in 0.75 mL of 1:10000 diluted goat anti-mouse IgG-HRP conjugated secondary antibody (DAKO) in wash buffer for 45 min at room temperature. The secondary antibody was removed, and the samples washed in 4 x 1 mL PBS for 20 min each wash. The samples were transferred to a new 24-well plate and 0.4 mL TMB solution (Thermo) added for 20 min at room temperature. 100 μL aliquots of solution were transferred to a clean 96-well plate and the absorbance was read at 652 nm (A_{652}) on a SPECTROstar Nano plate reader (BMG labtech). Values represent means of quadruplicate measurements ± standard deviation.

3.6. Scanning Electron Microscopy (SEM)

Samples were attached to metal SEM stubs using double-sided conductive carbon tape. They were coated with gold for 2.5 min at 20 mA using an Emitech K550 sputter coater. SEM images were obtained using a Camscan MX 2600 FEGSEM using an accelerating voltage of 10 kV and magnifications of 500x.

3.7. Tensile testing

Films were cut into 5 mm wide strips using a scalpel. The thickness of each sample was measured using a digital micrometer. Before extension, samples were soaked with deionised water until they became fully hydrated. Tensile testing was performed using a Hounsfield uniaxial tester with a 5 N load cell. Each composition was tested five times. A gauge length of 15 mm and an extension rate of 6 mm min^{-1} were used.

Strain values were measured using a laser on the testing rig. Force vs strain data were plotted to derive the stiffness at high strain, failure stress and failure strain of each material

(Supplementary Figure 1). The failure stress and failure strain were calculated using Equations 1 and 2, where σ is the applied stress in Pa, *F* is the applied force in N, *A* is the sample cross-sectional area in m^2 and ε is the strain of the material. The failure stress and strain were calculated from the highest force that was exerted on the sample before it failed and its equivalent strain.

$$Equation\ 1. \qquad \sigma_{fail} = \frac{F_{fail}}{A}$$

$$Equation\ 2. \qquad \varepsilon(dimensionless) = \frac{\varepsilon(in\%)}{100}$$

The stiffness was obtained by plotting a line of best fit onto the high strain linear portion of the force-strain curve. The stiffness, *E* in Pa, was derived from the gradient using Equation 3, where *m* is the gradient in N $\%^{-1}$ of the resultant force vs strain graph.

$$Equation\ 3. \qquad E = \frac{100m}{A}$$

To account for noise, average values from 5 force values were calculated, and each force value was set to an initial value of zero.

3.8. Cell Culture

HT1080 cells derived from a human fibrosarcoma were obtained from the European Collection of Animal Cell Cultures, Porton Down, UK. Rugli cells, derived from a rat glioma, were from Dr. J. Gavrilovic, University of East Anglia, UK. All cell lines were cultured on tissue culture plastic flasks maintained in a humidified incubator with 5 % CO_2 at 37 °C in Dulbecco's modified Eagle's medium (DMEM) containing 10 % (v/v) fetal bovine

serum and 1 % (v/v) streptomycin/penicillin (complete media). Once 70-80 % confluent the cells were passaged into new flasks at $1/10^{th}$ of the original cell density. Cells were prepared for cell adhesion, spreading or proliferation analysis by detaching from the cell culture flasks with 0.05 % (w/v) trypsin / 0.02 % (w/v) EDTA and re-suspending in an appropriate volume of DMEM or complete media.

3.9. Cell Adhesion analysis

Where stated, wells of tissue culture plates were coated with SE diluted from a 1 wt% stock solution to a final concentration of between 1 and 20 μg/mL or with 5 μg/mL of soluble collagen I (First Link (UK) Ltd.). The solutions were removed, the wells were washed 3x with PBS then non-specific adsorption to the film or well was blocked with 600 μL or 150 μL of 2% w/v bovine serum albumin (BSA) in phosphate buffered saline (PBS) for 24- or 96-well plates respectively. After 60 min at room temperature the wells were washed 3x with PBS then 400 μL or 100 μL of cells were added at a density of $1x10^6$ cells/mL in DMEM to 24- or 96-well plates respectively. The plates were incubated at 37 °C/5 % CO_2 for 1 h and non-adherent cells were removed with 3 PBS washes. 300 μL or 75 μL of lysis buffer (81 mM TriSodium Citrate, 31 mM Citric Acid, 0.1% v/v Triton X-100, 1.85 mg/mL p-nitrophenyl phosphate (PNP) substrate, pH 5.4) was added to 24- or 96-well plates respectively and incubated for 16 h at 4°C. Either 200 μL or 50 μL of 2 M sodium hydroxide solution was then added to 24- or 96-wells respectively. 100 μL of solution was transferred to a clean 96-well plate and the absorbance read at 405nm (A_{405}) on a SPECTROstar Nano plate reader (BMG labtech).

For inhibition assays, wells were SE or soluble collagen I coated then BSA blocked as for cell adhesion analysis. 12.5 μL of 40 mM EDTA (final concentration 5 mM), 80 mM α-

lactose (final concentration 10 mM), 80 mM β-lactose (final concentration 10 mM), and/or 80 µg/mL heparan sulphate (final concentration 10 µg/mL) in DMEM were added to each well. The volume in each well was made up to 50 µL then 50 µL of Rugli cells was added at a density of $2x10^6$ cell/mL (final density $1x10^6$ cell/mL) for 1 h at 37 °C/5 % CO_2. Loosely adherent cells were removed, and bound cells were detected using a PNP substrate as for cell adhesion analysis

Values are means of quadruplicate measurements ± standard deviation.

3.10. Cell spreading analysis

Films and soluble collagen coated wells were prepared in a 24-well plate then BSA blocked as for adhesion analysis. 400 µL of cells at a concentration of $3x10^5$ cells/mL in DMEM were added to each well and incubated at 37 °C/5 % CO_2 for 210 min for Rugli cells and 180 min for HT1080 cells. These time points were chosen as they represent the duration required to observe spreading onto the positive control, soluble collagen I coated, tissue culture wells. 100 µL of 25 % w/v glutaraldehyde stock solution was added to each well to achieve a final concentration of 5 % w/v then incubated at room temperature for 20 min. The fixed cells were washed with 3 x 1 mL PBS then permeabilised with 600 µL of 0.5 %w/v Triton X-100 in PBS for 5 min at room temperature. The samples were washed 3x with PBS then 600 µL of 0.01 % rhodamine phalloidin (Molecular Probes, made up to manufacturer's instructions) in PBS was added for 30 min at room temperature in the dark. After washing 3x with PBS the cell nuclei were stained with 600 µL of 3.5 µM DAPI in H_2O for 2 min then washed 3x with H_2O. The samples were mounted onto glass slides using Vectashield antifade mounting medium, sealed with nail varnish, and visualised on a Zeiss Observer Z1 fluorescent microscope using a 20x magnification objective lens. The cell area was obtained

by thresholding the rhodamine-phalloidin stained images and measuring the cell-derived fluorescent area in ImageJ. The cell number for each image was derived from the DAPI stained images by using the nucleus counter plug-in feature of ImageJ. To calculate the average cell area the total fluorescent area for each image was divided by corresponding cell number. Values represent means of 5 measurements ± standard deviation.

3.11. Cell growth

Samples in 48-well plates were sterilised using ultraviolet (UV) light for 20 min then blocked using 300 μL of filter-sterilised 2 %w/v BSA for 1 h at room temperature. 300 μL of cells were added at a density of $3.5x10^4$ cells/mL in complete media to each well. Plates were incubated at 37 °C/5 % CO_2 for 1, 2 or 4 days, at which point 75 μL of 25 % w/v glutaraldehyde stock solution was added to each well to achieve a final concentration of 5 % w/v for 20 mins at room temperature. The wells were washed 3x with PBS and then permeabilised for 5 min with 300 μL of 0.5 %w/v Triton X-100 in PBS. The wells were washed three times with PBS and 300 μL of 3.5μM DAPI in H_2O was added for 2 min in the dark. Following 3x H_2O washes the cell nuclei were visualised using a Zeiss Observer Z1 fluorescent microscope and a 10x objective lens. The number of nuclei per field of view, of a known area, were counted manually and expressed as a cell count/$mm^{2.}$ Values represent means of quadruplicate measurements ± standard deviation.

3.12. Elastin fluorescence microscopy

Films were BSA blocked as for adhesion analysis then incubated in 1:1000 mouse anti-elastin antibody (clone BA-4, Abcam, UK) in PBS for 1 h. The primary antibody was aspirated, washed 3xPBS then incubated in 1:500 AlexaFluor 594 conjugated donkey-anti-mouse secondary antibody (Jackson Immuno Research) for 1 hour. The samples were washed

3x with PBS then mounted onto glass slides using Vectashield mounting media and visualised on a Zeiss Observer Z1 fluorescent microscope.

3.13. Statistical analysis

Unless otherwise stated all error bars indicate standard deviations from the mean. Statistical significance was determined with a student t-test with unequal variance where N/S indicates >0.05, * indicates $p \leq 0.05$, ** indicates $p \leq 0.01$, *** indicates $p \leq 0.001$ and **** indicates $p \leq 0.0001$.

4. Results

4.1. Scaffold characterisation

Composites were generated by blending appropriate volumes of 1 %w/v CN or elastin to produce films with increasing, 25%, 50% or 75%, content of soluble (SE) or insoluble (IE) elastin. ELISA analysis using an elastin-specific antibody confirmed the presence of elastin in these resultant materials (Figure 1). This showed that the amount of elastin incorporated into the composite was proportional to the amount of elastin in the slurry. As these films were crosslinked, this indicates that the elastin component was retained during EDC/NHS crosslinking in 75% ethanol. Although the absorbance measurements were above background levels for all the composite materials, detection was approximately 2.5-fold higher for 75% SE compared to 75% IE containing composites. Therefore, although the same mass of elastin was added, the degree of elastin detection varied. This is presumably due to the fibrillar morphology of IE which, effectively prevents the antibody from accessing the centre of the elastic fibre. This theory was tested by anti-elastin fluorescent microscopy of the IE composite (Figure 2). Autofluorescence, due to the presence of a crosslinking tricarboxylic amino acid with pyridinium ring [41] was used to visualise the entire elastin inclusion. This was clearly visible throughout the entirety of the large IE inclusions (green in Figure 2). Conversely, detection by the BA-4 anti-elastin antibody was restricted to the periphery of these inclusions (red in Figure 2). This suggests that only a sub-proportion of the elastin in the IE containing scaffolds was accessible by the detection antibody which could explain the lower IE to SE detection by ELISA for same nominal mass of elastin. SEM was used to image the protein films to determine how the microstructure was affected by the addition of SE or IE (Figure 3). This shows that films composed exclusively of CN did not contain large fibres but instead implies a roughened morphology. Addition of IE resulted in the presence of

large 5–6 μm diameter inclusions, indicated by arrows in Figure 3. These inclusions were not evenly distributed with some agglomeration apparent. By comparison, the addition of SE to films resulted in a smooth and relatively featureless film.

Tensile testing of these films showed that all the material compositions possessed a J-shaped force-strain curve (example shown in Supplementary Figure 1) which is frequently observed in a wide range of soft tissues. These showed a general trend that addition of IE decreased the material stiffness (Figure 4A), however due to spread of values for the 100%CN samples this was not statistically significant. Conversely, SE increased the stiffness of the composites in a concentration dependent manner with a 3.3-fold increase in the modulus at 50% SE content ($p=0.0008$ against 100%CN). Values are not shown for 75% SE inclusion as these films were not sufficiently robust for analysis. The failure stress was unaffected by the addition of IE and increased by the addition of SE (Figure 4B). By contrast the failure strain increased with IE addition, particularly at the highest 75% elastin content ($p=0.0002$ against 100%CN), with a failure strain of ~21 % (Figure 4C). Addition of SE did not influence the failure strain. It should be noted that all of these materials were cross-linked with EDC/NHS as this is necessary for stability in cell culture conditions. As cross-linking is known to change the mechanical properties of collagen-based materials the same crosslinking parameters were utilised across all of the samples.

4.2. Cell adhesion

HT1080 and Rugli cells were chosen to analyse the cell binding properties of the elastin-collagen composite materials as they contain well defined collagen-binding integrins, utilising $\alpha_2\beta_1$ and $\alpha_1\beta_1$ respectively [16,42,43], but with potentially differing elastin binding capacity. To directly test the elastin-binding profile of these cell lines, adhesion to SE coated onto tissue culture plastic, was examined (Figure 5). These data show a dramatic difference in

the adhesive response between these lines. Whilst SE can support Rugli cell adhesion at a coating concentration of ≥2 μg/ml, little HT1080 cell adhesion was observed with SE coating concentrations of up to 20 μg/ml. Inhibition analysis using well-known elastin-receptor blocking molecules (EDTA, β-lactose and heparan sulphate for integrin, elastin binding protein and GAG-mediated adhesion respectively) showed that Rugli cell adhesion was blocked in the presence of EDTA (Figure 5C). By contrast α-lactose alone (a low-activity control for β-lactose) resulted in a slight decrease in elastin engagement, however when combined with β-lactose or heparan sulphate it did not alter the cellular response. When all four inhibitors were added in combination, the degree of cell adhesion was similar to EDTA inhibition alone, indicating an integrin-mediated cell binding mechanism in Rugli cells. Similarly, Rugli cell adhesion to soluble CN was inhibited by EDTA, but not lactose or heparan sulphate, highlighting an integrin-mediated response to collagen (Figure 5D). Therefore Rugli but not HT1080 cells can bind to elastin via integrin receptors, making comparison of these model cell lines a convenient method to delineate the contribution of collagen only (HT1080) and collagen-elastin (Rugli) in our elastin-collagen composites.

Both HT1080 and Rugli cells could adhere to films fabricated solely from insoluble CN (Figure 6) giving absorbance values of 0.84±0.12 and 0.65±0.10 respectively. It should be noted that the entire well surface was covered with the film material, ensuring that cell adhesion is solely through the film material. These absorbance values were higher than BSA coated control wells showing values of between 0.11±0.02 and 0.2±0.1 on a low-adhesion surface. Adhesion to CN films was lower than the soluble CN ($Abs._{405}$ 1.61±0.17 and 2.42±0.12) and tissue culture plastic controls ($Abs._{405}$ 1.5±0.04 and 2.27±0.11) for HT1080 and Rugli cells respectively. The addition of up to 50% SE markedly increased Rugli cell adhesion by over 2-fold. This showed significance ($p=0.007$) over the CN-only control. Consistent with the lack of SE adhesion, inclusion of SE did not significantly alter the degree

of HT1080 cell adhesion. Although data are shown for 75% SE inclusion, these films were not fully resistant to the washing regime employed to remove non-adherent cells, and so only fragments remained attached to the wells. As film fragmentation was a dominant effect, masking the cell-binding properties, the values from these samples are shown with a dashed line and are excluded from analysis here. IE inclusion increased the degree of Rugli cell adhesion by ~ 2-fold at 75% IE content. Again, this showed significance ($p=0.00034$) over the CN-only material. Interestingly IE inclusion increased HT1080 cell adhesions by ~ 1.6-fold, presumably due to changes in the mechanics, roughness or surface area.

4.3. Cell Spreading

A short-term cell morphological analysis was conducted to determine if the collagen-elastin composites could elicit appropriate cellular engagement to promote cell spreading. Supplementary Figures 2A and 2B show representative fluorescent microscopy images of rhodamine phalloidin stained actin (red) and DAPI stained nuclei (blue) for HT1080 and Rugli cells respectively. For IE containing films the IE fibres are non-specifically stained with DAPI, however the nuclei are still apparent due to their relative intensity and circularity. Consistent with our previous reports showing that EDC/NHS crosslinked collagen does not support cell spreading [9], HT1080 cells and Rugli cells both possessed a rounded morphology on CN-only films. Addition of IE did not affect Rugli cell spreading, regardless of the concentration added. Conversely SE addition resulted in the formation of thin cellular projections that were not observed on the CN-only films. This appeared independent of the SE concentration with a similar morphology on films composed of all SE densities. Similarly, HT1080 cell spreading was observed on films containing SE, which, qualitatively, appeared to be dependent upon the amount of elastin present. The addition of IE did not lead to HT1080 spreading with all cells being round at all IE concentrations. Both HT1080 and Rugli

cells possessed a spread morphology on the positive soluble CN I control and a rounded morphology on the negative BSA control.

Quantitative analysis of the cell area on each material (Figure 7) is consistent with the qualitative observations. This shows that the cell area is similar on both the CN-only films and BSA controls for both HT1080 (205±37 and 172±26 μm^2) and Rugli cells (186±11 and 179±14 μm^2), confirming a lack of spreading on EDC/NHS crosslinked collagen. Addition of SE dose dependently increased the HT1080 cell area to 362±52 μm^2 at 75% SE content. This was significantly different to the CN-only films ($p=0.00086$ at 75% SE). By comparison HT1080 cells possessed a cell area of between 157±18 and 198±15 μm^2 on all IE containing composites. The Rugli cell area was sensitive to SE, although this was similar for all SE densities with a cell area of between 206±9 and 329±57 μm^2. This showed significance against the CN-only films ($p=0.0053$ at 75% SE). The Rugli cell area was insensitive to IE addition with cell areas of between 166±7 and 195±11 μm^2 for all compositions. Both cells lines spread onto soluble CN coated glass with cell areas of 627±70 and 512±51 μm^2 for HT1080 and Rugli cells respectively.

4.4. Cell proliferation

We have previously shown that a loss of divalent cation-dependent cell adhesion to EDC/NHS crosslinked insoluble CN I inhibits cell proliferation [9]. As SE and IE incorporation alters the cell adhesive properties of collagen-based materials, we have measured cell proliferation on SE and IE composites (Figure 8). Both cell lines could proliferate on a positive soluble CN I coated control, with the number of cells/mm^2 of material increasing ~6- and ~ 18-fold over 4 days in culture for HT1080 and Rugli cells respectively. This confirms the proliferative capacity of these cells.

Consistent with our previous observations, HT1080 cells did not proliferate on EDC/NHS crosslinked CN-only films with ~40-50% fewer cells at day 4 compared to day 1. Inclusion of IE or SE had no significant effect on HT1080 cell proliferation over the no-elastin controls. For example, there were ~50 and 40% fewer cells after 4 days in culture on 75% IE and 75% SE containing samples respectively. Rugli cells showed low levels of cell proliferation on CN-only samples with an approximately 4-fold increase in the cell density between day 1 and day 4 in culture. This was significantly below the ~18-fold increase in cell number observed on the soluble CN I control. Therefore, although Rugli cells showed proliferative capacity on EDC/NHS crosslinked CN, this was ~ 4-5 times lower than for non-crosslinked collagen. Interestingly, inclusion of IE and SE could dose-dependently increase the proliferative response of Rugli cells. This showed significance over the CN-only control with $p=0.0032$ and 0.00017 for 75% SE and 75% IE containing films respectively. Rugli proliferation was noticeably higher on the SE compared to IE composites. This was evident at all densities of elastin inclusion. For example, inclusion of 25%, 50% or 75% IE resulted in a ~4-, 7- or 12-fold increase in the cell number between day 1 and day 4. By comparison inclusion of 25%, 50% or 75% SE resulted in a ~6-, 16- and 16-fold increase in the Rugli cell number over the same duration. Indeed with 75% SE incorporation the degree of cell proliferation was approaching that observed on the soluble CN I positive control. Therefore, elastin incorporation can selectively increase the proliferation of cell types that possess the appropriate elastin-binding receptors.

5. Discussion

Matching the mechanical and biochemical properties of soft tissue implants to the surrounding tissue is functionally important [44,45]. As major components of numerous soft tissues, IE and SE, in combination with CN, was investigated. Analysis of these composites showed that the mechanical and cell-ligating properties of CN-based materials can be tailored by incorporating elastin. Furthermore, by comparing 2 complementary cell lines, one of which utilises elastin-binding receptors, and the other which does not, we determined the influence of elastin- and CN-receptor engagement on the cell response over short-term (adhesion, spreading) and long-term (proliferation) culture.

J-shaped force-strain plots were observed for all films, in which the gradient of the force-strain profile increases with strain. The initial extension phase of this profile is presumably dominated by CN fibril realignment towards the tensile axis, after which further extension is via the stiffer CN fibres. These profiles yielded stiffness values that are comparable to the literature values of 2–31 MPa, depending on the composition [18,36]. In our hands, inclusion of up to 75% IE decreased the stiffness and failure stress of films but increased the failure strain. This is consistent, to a reasonable approximation, with disruption of the CN network by the large and discrete IE inclusions [18]. By comparison SE had the opposite effect to IE inclusion. SE was spread across the entire CN film, without large inclusions, and so it is possible that the SE component resisted the applied force in parallel with the CN. Our data contradicts others showing that SE decreased the stiffness of CN-based films, however, the differing fabrication processes [36] and elastin concentration [18] prevent direct extrapolation. No significant influence on the yield strain was observed with up to 50% IE or SE content, agreeing with CN-based films manufactured using electrochemical alignment [36]. Interestingly we observed an increase in the yield strain with 75% IE

inclusion, presumably as the loading was resisted by the IE component. Alternatively, it is possible that the physical properties are due to the lower CN content upon increasing addition of IE or SE to the total 1% w/v slurry protein content. This fits well with the lack of IE or SE influence on the failure strain as the alignment and tensile stretch of each CN fibre does not change with lower CN density. However this cannot describe the differences between SE and IE composites. Therefore, it is likely that there is a complex interplay between the distribution and density these components, with different intrinsic mechanical properties. Others have used electrospinning to further refine the physical properties of elastin-CN composites, however the architectural properties of these fibres heavily influence cell behaviour, and so amorphous blended films were chosen here to reduce the number of interconnected parameters, allowing direct comparison to the cell response.

Currently the cell-binding properties of CN-elastin composites are relatively poorly understood. Although elastin addition influences smooth muscle cell behaviour on CN-based materials [31,35], the contribution from the elastin and CN component is unknown. The major aim of this study was to explore this complex fundamental interplay by assigning the cellular response to the CN and elastin elements. Our approach was to compare two different model cell lines, one of which utilises elastin binding receptors and the other which is insensitive to elastin. For this reason HT1080 and Rugli cells were chosen as they have well described CN-binding receptors ($\alpha_2\beta_1$ and $\alpha_1\beta_1$ respectively [13]) and the influence that EDC crosslinking exerts on their response to CN-only films is known [9]. We therefore examined the elastin-binding capacity of each on SE coated tissue culture plastic. SE solution was chosen over IE suspension to enable careful control over the coating concentration. This analysis clearly showed that Rugli, but not HT1080 cells, could adhere to SE in an EDTA-sensitive manner, suggesting integrin-dependence of Rugli adhesion. We should point out that enzymatic-based cell detection, and not cell staining, was used here to avoid high non-

specific, collagen-film-associated, background values. Although we cannot entirely preclude the possibility that the materials affect the cell-derived enzymatic activity, cell number linear regressions and microscopic observations were used to control for this possibility. As such enzymatic detection of these cell lines was used to examine a series of IE and SE-collagen composites.

Consistent with EDC-induced modulation of cell adhesion, spreading and proliferation on CN-based materials, both Rugli and HT1080 cell adhesion to CN-only films was lower than a soluble CN I control. This has been attributed to EDC-dependent blocking of native-like integrin binding to critical carboxylic acid side chains in GxOGER motifs, and induction of non-native cell binding mechanisms that do not support cell proliferation [9]. Therefore, it highly likely that adhesion on the CN-only films was non-native, which correlates well to the subsequent lack of cell spreading and proliferation.

Inclusion of elastin into collagen films affects numerous different cell-responsive facets simultaneously, including the availability of cell-binding motifs, roughness and stiffness. Comparison of Rugli against HT1080 cells allowed us to deconvolute the contribution of elastin-derived cell-adhesive motifs. The Rugli response was dramatically altered by the addition of elastin to collagen-based materials with increased attachment, spreading and particularly pronounced proliferation. The integrin-dependent SE-binding mechanism of Rugli cells indicate that elastin-derived integrin-binding motifs within elastin promote this potent biological effect. These could include the integrin-binding motifs RKRK and AAAAAAAAAAKAAKYGAAAGL [26] that ligate with integrins $\alpha_V\beta_3$ and $\alpha_V\beta_5$ [24,25]. However there are reports that the C-terminal region of the elastin monomer, tropoelastin, may be lost in mature elastic fibres [46]. As such it is possible that the C-terminal RKRK motif integrin binding site may be absent in our elastin-collagen composites. In addition, although amino acid analysis indicates that collagen and elastin are the major

constituent of our protein preparations (Supplementary Figure 3), we cannot completely discount the possibility that each could contain traces of other bioactive molecules. For example, microfibril-associated glycoprotein can contaminate elastin preparations. Notwithstanding these caveats, our data clearly show that elastin addition offers huge potential to integrate cell-biological activity in to EDC/NHS crosslinked CN-based materials.

The Rugli cell response was modulated by both IE and SE, however by mass, SE promoted increased cell adhesion, spreading and proliferation than IE. Interestingly this trend is similar to the degree of BA-4 detection by ELISA. One possible explanation is the innate, densely packed, fibrous architecture of IE, where the elastin molecules within the fibre core are not solvent accessible. This was clearly evident from anti-elastin fluorescent microscopy of IE samples. As a large proportion of the elastin mass in the IE films is not available for cell engagement, comparing the cellular response against elastin mass potentially under-represents the bio-activity of the IE component. Instead Rugli proliferation and attachment correlate linearly with SE and IE detection (R^2 between 0.992 and 0.882) by ELISA (Figure 10). When compared in this manner, the cellular response to the IE and SE addition are very similar. This is particularly important as the other characteristics of IE and SE containing films, such as mechanical properties and roughness profiles, do not correlate with the cellular response. Instead, once the relative solvent exposure is accounted for, the Rugli response is, predominated by the elastin inclusions.

We have shown that HT1080 cells do not adhere to elastin. Despite this HT1080 cell adhesion and spreading were elevated with the inclusion of SE but not IE. Whilst it is unlikely that this response is through direct cell-anchorage to elastin, it could be via SE-modulation of the collagen component and/or via the physical properties of the material. For example, it is possible that elastin alters EDC-dependent inhibition of collagen-cell interactions [9] due to altered stoichiometry of the crosslinking reaction by the amine-rich

regions on elastin. Alternatively, the influence of SE on the mechanical properties and roughness could alter the cellular response. As the mechanical properties and chemistry of the CN films change in tandem with SE addition these two explanations cannot be separated here. It should also be noted that the relevance of bulk mechanical properties to cell behaviour is often not a simple correlation as the small-scale stiffness sensed by the cells is not necessarily the same as the bulk stiffness measured by stress-strain techniques. It is also possible that SE addition alters the collagen spacing (i.e. by separating collagen fibres) which influences the cell response. One surprising finding was that elastin inclusion induced HT1080 cell spreading. Although we have shown that HT1080 cells do not adhere to elastin, it is possible that elastin is engaging with signalling molecules on these cells. One such example is the elastin binding protein which would not possess sufficient affinity to support cell adhesion but has been shown to activate signalling cascades [47,48].

SE or IE inclusion dramatically increased Rugli but not HT1080 cell proliferation. This differential response between the cell lines suggests that the cell proliferative response is not solely due to the CN component or physical attributes of the films as these would influence both cell lines similarly. Instead it is likely elastin-binding integrin-associated signalling cascades promote cell proliferation [49].

In summary, comparison of two independent cell lines, each with a differing affinity for elastin have shown that addition of elastin-specific cell-binding motifs, or modulation of the CN component in an elastin-CN composite both contribute to the ultimate cellular response. Moreover, for cells that possess elastin-binding integrins, the elastin component can dominate over the EDC crosslinked CN component leading to a cell-inductive long-term response.

6. Conclusion

SE and IE were successfully incorporated into CN-based materials. Both SE and IE significantly altered the mechanical properties of CN-based films where SE increased but IE decreased the stiffness and failure stress. Two cell lines were identified which possessed differing elastin-binding properties. These allowed delineation of the cellular response to the CN and elastin components of the composites. The solvent accessibility of the elastin element of the films heavily influenced the behaviour of cells which possessed elastin-binding integrins. By comparison, if cells were devoid of elastin-binding integrins then it was the indirect influence of elastin, over the physical properties and CN component, that dictated the cellular response. Therefore, we have established that the cellular response to CN-elastin composites is highly dependent upon the cell surface receptor expression profile. CN and elastin are the most abundant protein components of tissues and are ubiquitously employed for tissue engineering. Consequently, these data offer the opportunity to control the bioactivity that each of the components bestows upon these complex *heterogeneous* materials.

7. Acknowledgements

This work was supported by the ERC Advanced Grant 320598 3D-E, EPSRC fellowship EP/N019938/1, and British Heart Foundation Special Project SP/15/7/31561 D. V. Bax was funded by the Peoples Programme of the EU 7th Framework Programme (RAE no: PIIF-GA-2013-624904).

8. References

[1] C.H. Lee, A. Singla, Y. Lee, Biomedical applications of collagen., Int. J. Pharm. 221 (2001) 1–22.

[2] L.C. Abraham, E. Zuena, B. Perez-Ramirez, D.L. Kaplan, Guide to collagen characterization for biomaterial studies., J. Biomed. Mater. Res. B. Appl. Biomater. 87 (2008) 264–285.

[3] L.H. Olde Damink, P.J. Dijkstra, M.J. van Luyn, P.B. van Wachem, P. Nieuwenhuis, J. Feijen, Cross-linking of dermal sheep collagen using a water-soluble carbodiimide., Biomaterials. 17 (1996) 765–773.

[4] L. Buttafoco, P. Engbers-Buijtenhuijs, A.A. Poot, P.J. Dijkstra, W.F. Daamen, T.H. van Kuppevelt, I. Vermes, J. Feijen, First steps towards tissue engineering of small-diameter blood vessels: preparation of flat scaffolds of collagen and elastin by means of freeze drying., J. Biomed. Mater. Res. B. Appl. Biomater. 77 (2006) 357–368.

[5] I. Rault, V. Frei, D. Herbage, N. Abdul-Malak, A. Huc, Evaluation of different chemical methods for cross-linking collagen gel, films and sponges, J. Mater. Sci. Mater. Med. 7 (1996) 215–221.

[6] C.N. Grover, J.H. Gwynne, N. Pugh, S. Hamaia, R.W. Farndale, S.M. Best, R.E. Cameron, Crosslinking and composition influence the surface properties, mechanical stiffness and cell reactivity of collagen-based films, Acta Biomater. 8 (2012) 3080–3090.

[7] C.N. Grover, R.E. Cameron, S.M. Best, Investigating the morphological, mechanical and degradation properties of scaffolds comprising collagen, gelatin and elastin for use in soft tissue engineering, J. Mech. Behav. Biomed. Mater. 10 (2012) 62–74.

[8] N. Davidenko, T. Gibb, C. Schuster, S.M. Best, J.J. Campbell, C.J. Watson, R.E. Cameron, Biomimetic collagen scaffolds with anisotropic pore architecture, Acta Biomater. 8 (2012) 667–676.

[9] D. V. Bax, N. Davidenko, D. Gullberg, S.W. Hamaia, R.W. Farndale, S.M. Best, R.E. Cameron, Fundamental insight into the effect of carbodiimide crosslinking on cellular recognition of collagen-based scaffolds, Acta Biomater. 49 (2017) 218–234.

[10] D. Sheppard, The role of integrins in pulmonary fibrosis, Eur. Respir. Rev. 17 (2008) 157–162.

[11] J.D. Humphries, A. Byron, M.J. Humphries, Integrin ligands at a glance, J. Cell Sci. 119 (2006) 3901–3903.

[12] M. Barczyk, S. Carracedo, D. Gullberg, Integrins, Cell Tissue Res. 339 (2010) 269–280.

[13] S. Hamaia, R.W. Farndale, Integrin recognition motifs in the human collagens, Adv. Exp. Med. Biol. 819 (2014) 127–142.

[14] R.W. Farndale, T. Lisman, D. Bihan, S. Hamaia, C.S. Smerling, N. Pugh, A. Konitsiotis, B. Leitinger, P.G. de Groot, G.E. Jarvis, N. Raynal, Cell–collagen interactions: the use of peptide Toolkits to investigate collagen–receptor interactions, Biochem. Soc. Trans. 36 (2008) 241–250.

[15] P.R.-M. Siljander, S. Hamaia, A.R. Peachey, D.A. Slatter, P.A. Smethurst, W.H. Ouwehand, C.G. Knight, R.W. Farndale, Integrin activation state determines selectivity for novel recognition sites in fibrillar collagens, J. Biol. Chem. 279 (2004) 47763–47772.

[16] C.G. Knight, L.F. Morton, A.R. Peachey, D.S. Tuckwell, R.W. Farndale, M.J. Barnes, The collagen-binding A-domains of integrins alpha(1)beta(1) and alpha(2)beta(1) recognize the same specific amino acid sequence, GFOGER, in native (triple-helical) collagens., J. Biol. Chem. 275 (2000) 35–40.

[17] J. Emsley, C.G. Knight, R.W. Farndale, M.J. Barnes, R.C. Liddington, Structural Basis of Collagen Recognition by Integrin α2β1, Cell. 101 (2000) 47–56.

[18] C.N. Grover, R.W. Farndale, S.M. Best, R.E. Cameron, The interplay between physical and chemical properties of protein films affects their bioactivity, J. Biomed. Mater. Res. Part A. 100 (2012) 2401–2411.

[19] J.-D. Malcor, D. Bax, S.W. Hamaia, N. Davidenko, S.M. Best, R.E. Cameron, R.W. Farndale, D. Bihan, The synthesis and coupling of photoreactive collagen-based peptides to restore integrin reactivity to an inert substrate, chemically-crosslinked collagen, Biomaterials. 85 (2016) 65–77.

[20] J. Uitto, Biochemistry of the elastic fibers in normal connective tissues and its alterations in diseases, J. Invest. Dermatol. 72 (1979) 1–10.

[21] R.P. Mecham, A. Hinek, R. Entwistle, D.S. Wrenn, G.L. Griffin, R.M. Senior, Elastin binds to a multifunctional 67-kilodalton peripheral membrane protein, Biochemistry. 28 (1989) 3716–3722.

[22] R.M. Senior, G.L. Griffin, R.P. Mecham, D.S. Wrenn, K.U. Prasad, D.W. Urry, Val-Gly-Val-Ala-Pro-Gly, a repeating peptide in elastin, is chemotactic for fibroblasts and monocytes., J. Cell Biol. 99 (1984) 870–874.

[23] T.J. Broekelmann, B.A. Kozel, H. Ishibashi, C.C. Werneck, F.W. Keeley, L. Zhang, R.P. Mecham, Tropoelastin interacts with cell-surface glycosaminoglycans via its COOH-terminal domain., J. Biol. Chem. 280 (2005) 40939–40947.

[24] D. V. Bax, U.R. Rodgers, M.M.M. Bilek, A.S. Weiss, Cell Adhesion to Tropoelastin Is Mediated via the C-terminal GRKRK Motif and Integrin $\alpha_V \beta_3$, J. Biol. Chem. 284 (2009) 28616–28623.

[25] P. Lee, D. V. Bax, M.M.M. Bilek, A.S. Weiss, A novel cell adhesion region in tropoelastin mediates attachment to integrin αVβ5, J. Biol. Chem. 289 (2014) 1467–1477.

[26] P. Lee, G.C. Yeo, A.S. Weiss, A cell adhesive peptide from tropoelastin promotes sequential cell attachment and spreading via distinct receptors, FEBS J. 284 (2017) 2216–2230.

[27] J.F. Almine, D. V. Bax, S.M. Mithieux, L. Nivison-Smith, J. Rnjak, A. Waterhouse, S.G. Wise, A.S. Weiss, Elastin-based materials, Chem. Soc. Rev. 39 (2010) 3371–3379.

[28] J. Rnjak, Z. Li, P.K.M. Maitz, S.G. Wise, A.S. Weiss, Primary human dermal fibroblast interactions with open weave three-dimensional scaffolds prepared from synthetic human elastin, Biomaterials. 30 (2009) 6469–6477.

[29] Q. Lu, K. Ganesan, D.T. Simionescu, N.R. Vyavahare, Novel porous aortic elastin and collagen scaffolds for tissue engineering., Biomaterials. 25 (2004) 5227–5237.

[30] D.T. Simionescu, Q. Lu, Y. Song, J.S. Lee, T.N. Rosenbalm, C. Kelley, N.R. Vyavahare, Biocompatibility and remodeling potential of pure arterial elastin and collagen scaffolds., Biomaterials. 27 (2006) 702–713.

[31] A.J. Ryan, F.J. O'Brien, Insoluble elastin reduces collagen scaffold stiffness, improves viscoelastic properties, and induces a contractile phenotype in smooth muscle cells.,

Biomaterials. 73 (2015) 296–307.

[32] J. Rnjak-Kovacina, S.G. Wise, Z. Li, P.K.M. Maitz, C.J. Young, Y. Wang, A.S. Weiss, Tailoring the porosity and pore size of electrospun synthetic human elastin scaffolds for dermal tissue engineering, Biomaterials. 32 (2011) 6729–6736.

[33] C.B. Saitow, S.G. Wise, A.S. Weiss, J.J. Castellot, D.L. Kaplan, Elastin biology and tissue engineering with adult cells, Biomol. Concepts. 4 (2013) 173–185.

[34] W.F. Daamen, S.T.M. Nillesen, T. Hafmans, J.H. Veerkamp, M.J.A. van Luyn, T.H. van Kuppevelt, Tissue response of defined collagen-elastin scaffolds in young and adult rats with special attention to calcification., Biomaterials. 26 (2005) 81–92.

[35] W.F. Daamen, H.T.B. van Moerkerk, T. Hafmans, L. Buttafoco, A.A. Poot, J.H. Veerkamp, T.H. van Kuppevelt, Preparation and evaluation of molecularly-defined collagen-elastin-glycosaminoglycan scaffolds for tissue engineering., Biomaterials. 24 (2003) 4001–4009.

[36] T.-U. Nguyen, C.A. Bashur, V. Kishore, Impact of elastin incorporation into electrochemically aligned collagen fibers on mechanical properties and smooth muscle cell phenotype., Biomed. Mater. 11 (2016) 025008.

[37] A. Waterhouse, S.G. Wise, M.K.C. Ng, A.S. Weiss, Elastin as a nonthrombogenic biomaterial., Tissue Eng. Part B. Rev. 17 (2011) 93–99.

[38] J. Skopinska-Wisniewska, A. Sionkowska, A. Kaminska, A. Kaznica, R. Jachimiak, T. Drewa, Surface characterization of collagen/elastin based biomaterials for tissue regeneration, Appl. Surf. Sci. 255 (2009) 8286–8292.

[39] G. Lammers, G.S. Tjabringa, J. Schalkwijk, W.F. Daamen, T.H. van Kuppevelt, A molecularly defined array based on native fibrillar collagen for the assessment of skin tissue engineering biomaterials., Biomaterials. 30 (2009) 6213–6220.

[40] S.M. Partridge, H.F. Davis, G.S. Adair, The chemistry of connective tissues. 2. Soluble proteins derived from partial hydrolysis of elastin., Biochem. J. 61 (1955) 11–21.

[41] Z. Deyl, K. Macek, M. Adam, O. Vancíková, Studies on the chemical nature of elastin fluorescence., Biochim. Biophys. Acta. 625 (1980) 248–254.

[42] N. Raynal, S.W. Hamaia, P.R.-M. Siljander, B. Maddox, A.R. Peachey, R. Fernandez, L.J. Foley, D.A. Slatter, G.E. Jarvis, R.W. Farndale, Use of synthetic peptides to locate novel integrin alpha2beta1-binding motifs in human collagen III, J. Biol. Chem. 281 (2006) 3821–3831.

[43] S. Perret, J.A. Eble, P.R.-M. Siljander, C. Merle, R.W. Farndale, M. Theisen, F. Ruggiero, Prolyl hydroxylation of collagen type I is required for efficient binding to integrin alpha 1 beta 1 and platelet glycoprotein VI but not to alpha 2 beta 1., J. Biol. Chem. 278 (2003) 29873–29879.

[44] J.D. Berglund, R.M. Nerem, A. Sambanis, Viscoelastic testing methodologies for tissue engineered blood vessels., J. Biomech. Eng. 127 (2005) 1176–1184.

[45] T. Sugiura, R. Agarwal, S. Tara, T. Yi, Y.-U. Lee, C.K. Breuer, A.S. Weiss, T. Shinoka, Tropoelastin inhibits intimal hyperplasia of mouse bioresorbable arterial vascular grafts, Acta Biomater. 52 (2017) 74–80.

[46] T. Broekelmann, C. Ciliberto, A. Shifren, R. Mecham, Modification and functional inactivation of the tropoelastin carboxy-terminal domain in cross-linked elastin, Matrix Biol. 27 (2008) 631–639.

[47] S. Mochizuki, B. Brassart, A. Hinek, Signaling pathways transduced through the elastin receptor facilitate proliferation of arterial smooth muscle cells, J. Biol. Chem. 277 (2002) 44854–44863.

[48] M. Donet, S. Brassart-Pasco, S. Salesse, F.-X. Maquart, B. Brassart, Elastin peptides regulate HT-1080 fibrosarcoma cell migration and invasion through an Hsp90-dependent mechanism., Br. J. Cancer. 111 (2014) 139–148.

[49] P. Moreno-Layseca, C.H. Streuli, Signalling pathways linking integrins with cell cycle progression, Matrix Biol. 34 (2014) 144–153.

9. Figure legends

Figure 1 : Enzyme linked immunosorbent analysis of the elastin content of IE- (light grey bars) and SE- (dark grey bars) containing CN films as detected by the BA-4 anti-elastin antibody (y-axis). The composite composition in relative % composition is detailed on the x-axis. The negative control indicates a no-film reference sample (unfilled bar). Error bars indicate S.D. of quadruplicate measurements.

Figure 2 : Phase contrast microscopy (**A**) and fluorescent microscopy (**B-D**) of 75%IE-25%CN composites. Autoflorescence of the IE fibres [41] is shown in (**B**) and green in the merged image (**D**). BA-4 anti-elastin antibody detection is shown in (**C**) and red in the merged image (**D**). Arrows highlight peripheral antibody detection on IE fibres in (**D**). The scale bar indicates 200μm.

Figure 3 : Scanning Electron Micrographs of CN only (**A**), CN-IE (**B**) and CN-SE composites (**C**). The composition is shown as a relative % of each component. Arrows highlight IE inclusions. Scale bar indicates 50μm.

Figure 4 : Stiffness (**A**), failure stress (**B**) and failure strain (**C**) of CN-IE (**i**) or CN-SE composites (**ii**). The relative % of collagen and elastin is shown on the x-axis. No data are shown for 25%CN-75%SE films as these adhered to the mould and could not be removed for analysis. Error bars indicate S.D. (n=5). N/S, * and *** indicate >0.05, <0.05, <0.001 significance from the 100%CN/0%elastin values respectively.

Figure 5 : HT1080 (**A**) or Rugli (**B**) cell adhesion to SE coated onto tissue culture plastic surfaces. The coating concentration of SE is shown on the x-axis and cell derived absorbance on the y-axis. Bovine serum albumin (BSA) was used to block non-specific adhesion to the tissue culture plastic substrate. The degree of non-specific adhesion to BSA is shown with a dashed line. Inhibition of Rugli cell adhesion to SE (**C**) or soluble CN (**D**) using EDTA (inhibits integrins), β-lactose (β-lac; inhibits elastin binding protein), α-lactose (α-lac; non-functional control for β-lactose) and heparan sulphate (H/S; inhibits GAG binding). The inhibitor inclusion is detailed under the x-axis. Error bars indicate S.D. of quadruplicate measurements. N/S, *, **, *** and **** indicate >0.05, <0.05, <0.01, <0.001 and <0.0001 significance from the 0 μg/ml SE values (**A,B**) or no-inhibitor controls (**C,D**) respectively.

Figure 6 : HT1080 (**A**) or Rugli (**B**) cell adhesion to CN films containing an increasing content of SE (blue, cross) or IE (red, diamond). The relative % of CN or elastin is shown on the x-axis and cell derived absorbance is on the y-axis. Adhesion to 25%CN-75% SE films is shown with a dashed cross and line as these composites fragmented during the washing regime used to remove loosely bound cells. Non-specific adhesion was blocked with bovine serum albumin (BSA) for all composites. Cell binding to 5 μg/ml soluble CN I coated tissue culture plastic (square), tissue culture plastic (circle) and the negative control BSA-blocked tissue culture plastic (triangle) are shown in grey. Error bars indicate S.D. of quadruplicate measurements. N/S, ** and *** indicate >0.05, <0.01 and <0.001 significance from the 100%CN-0% elastin values respectively.

Figure 7 : Cell area quantification for HT1080 (**A**) or Rugli (**B**) cells on films with increasing SE (blue bars) or IE (red bars) content. The relative % CN and elastin content is shown beneath each pair of bars. Non-specific adhesion was blocked with bovine serum albumin (BSA). The cell area on a negative control (BSA), a positive control (5 μg/ml soluble CN I coated glass) and CN-only films are shown with grey bars. Error bars indicate S.D. (n=5). N/S, **, *** and **** indicate >0.05, <0.01, <0.001 and <0.0001 significance when compared to the 100%CN-0% elastin values respectively.

Figure 8 : Cell count over 4 days in culture for HT1080 (**A,B**) and Rugli (**C,D**) cells on SE (**B,D**) or IE (**A,C**) containing composites. The relative % CN and elastin content is identical for all graphs and the legend is shown at the bottom of the figure. A 5 μg/ml soluble CN I coated tissue culture plastic positive control is shown (black, cross). Error bars indicate S.D. of quadruplicate measurements. N/S, **, *** and **** indicate >0.05, <0.01, <0.001 and <0.0001 significance when compared to the 100%CN-0% elastin values at Day 4.

Figure 9 : Direct comparison of the degree of SE (**C,D**) and IE (**A,B**) detection by ELISA analysis (x-axis - taken from Figure 1) and Rugli cell count at Day 4 (**A,C** – y-axis - taken from Figure 8) or adhesion (**B,D** – y-axis - taken from Figure 6). Associated background values on the bovine serum albumin negative controls were deducted for all values. Linear regressions fit with R^2 values of 0.992 (**A**), 0.955 (**B**), 0.882 (**C**), 0.9386 (**D**).

Supplementary figure 1 : Representative force versus strain tensile test profiles for collagen-elastin films. The red dashed lines indicate the calculation of failure force and failure strain. The green line shows the gradient used to derive stiffness.

Supplementary figure 2 : Rhodamine-phalloidin (actin assembly; red) and DAPI (cell nuclei; blue) stained fluorescent microscopy of HT1080 (**A**) or Rugli cells (**B**). The relative % composition of CN or elastin is stated for each micrograph. Non-specific interaction was blocked with bovine serum albumin (BSA) for all conditions. The positive control, 5 μg/ml soluble CN I, and negative control, BSA, are shown for reference. The scale bar indicates 100μm.

Supplementary figure 3 : Amino acid content of elastin (**A**) or soluble CN (**B**) used to fabricate films. SE is shown in blue, IE in red and CN in black. Predicted amino acid content, derived from the primary amino acid sequences is shown in grey. Threonine, Serine and Methionine are not shown due to small amounts of degradation during analysis. Lysine and Proline are not shown due to post-translational modification.

Figure 1

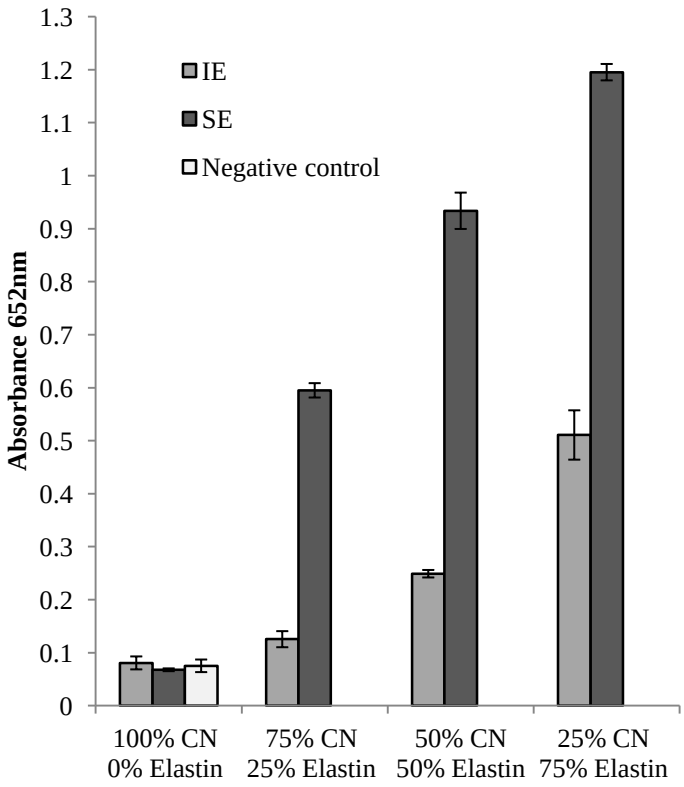
1.3
1.2
1.1
1
0.9
0.8
0.7
0.6
0.5
0.4
0.3
0.2
0.1
0
Absorbance 652nm
IE
SE
Negative control
100% CN
0% Elastin
75% CN
25% Elastin
50% CN
50% Elastin
25% CN
75% Elastin

Figure 2

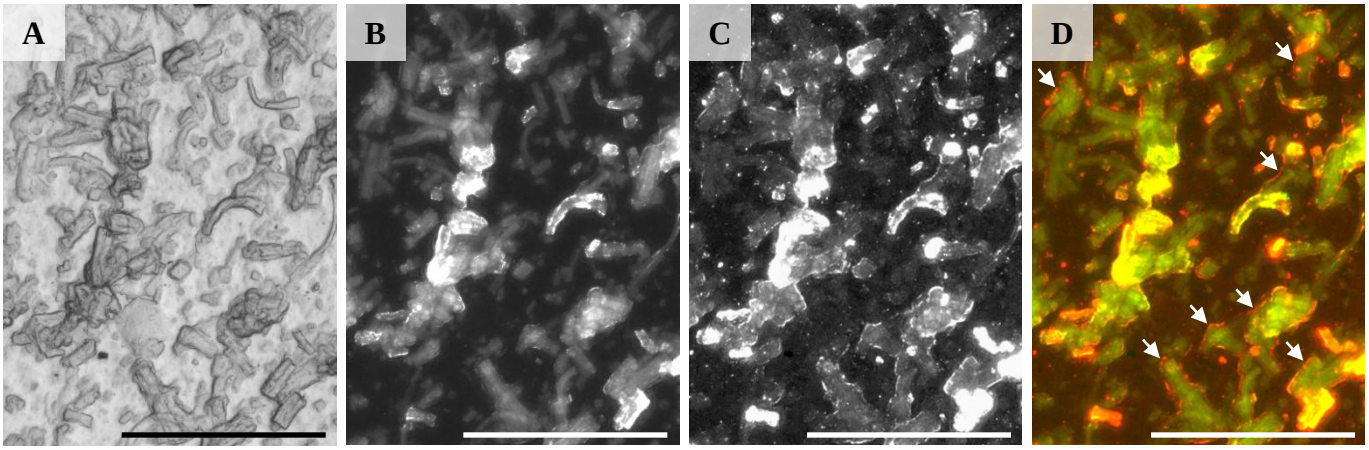

Figure 3

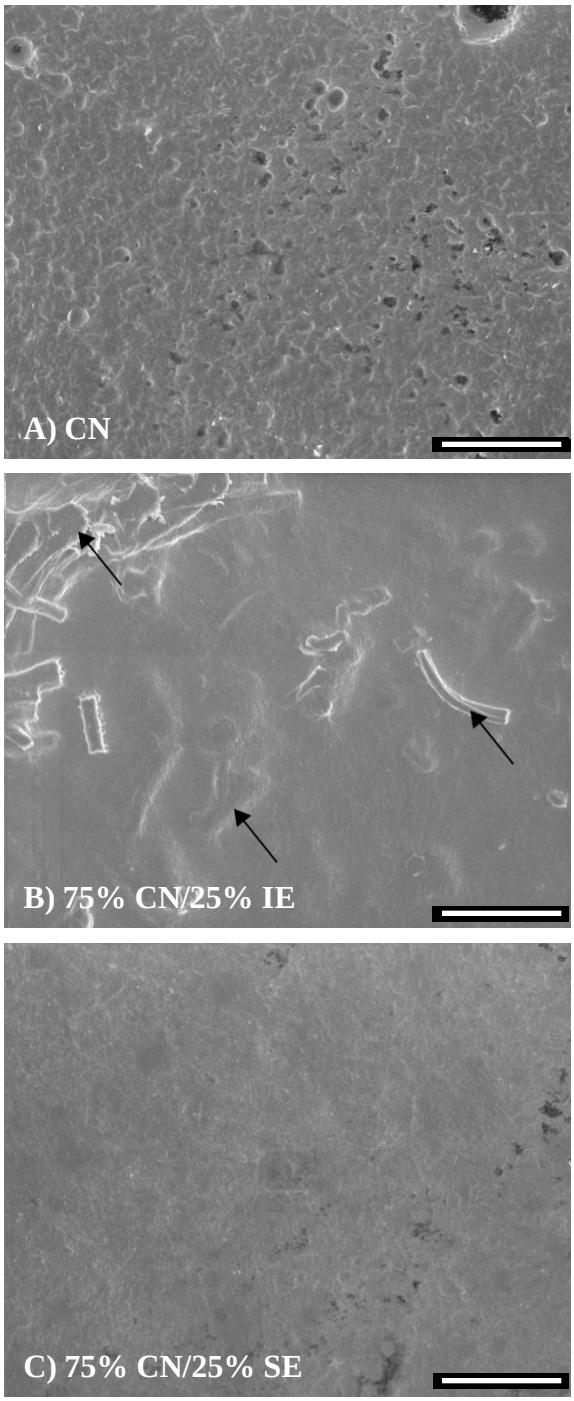

Figure 4

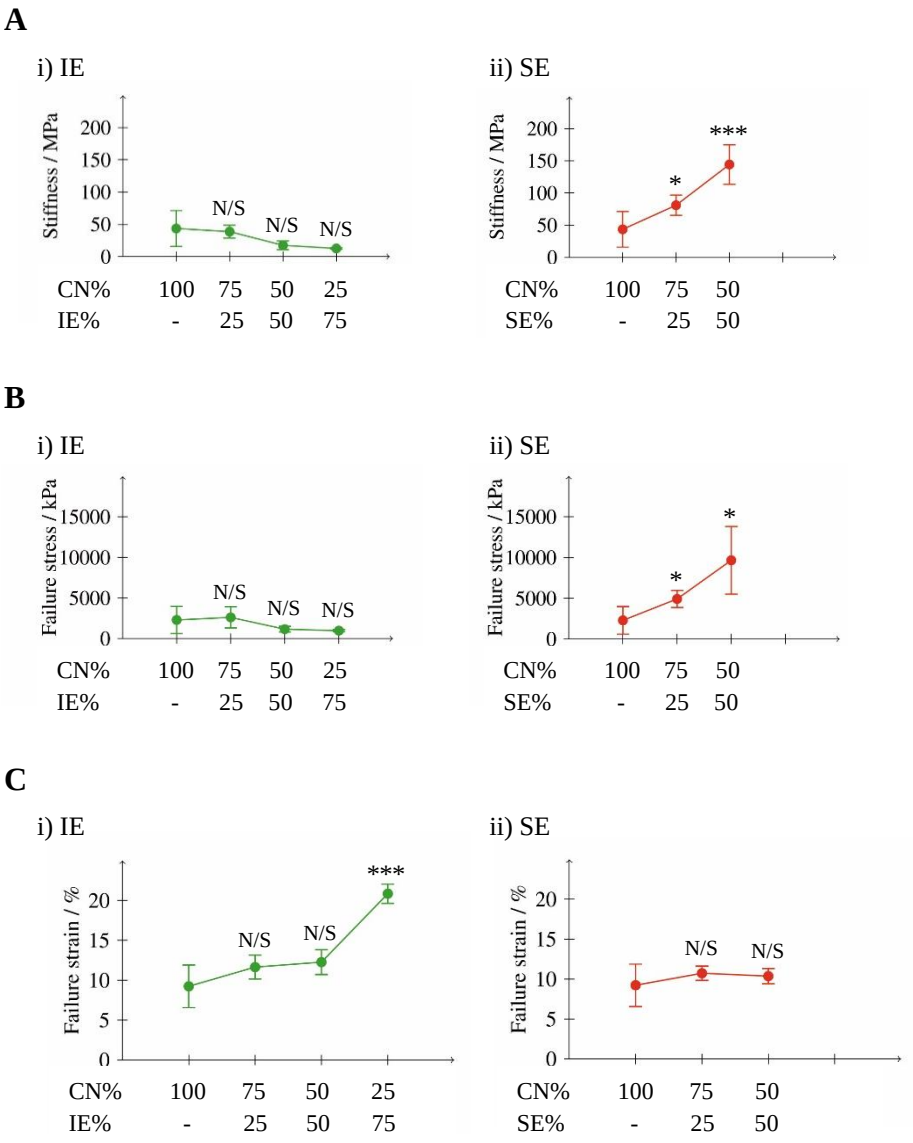
A
i) IE
Stiffness / MPa
200
150
100
50
0
N/S
N/S
N/S
CN% 100 75 50 25
IE% - 25 50 75
ii) SE
Stiffness / MPa
200
150
100
50
0
*
***
CN% 100 75 50
SE% - 25 50
B
i) IE
Failure stress / kPa
15000
10000
5000
0
N/S
N/S
N/S
CN% 100 75 50 25
IE% - 25 50 75
ii) SE
Failure stress / kPa
15000
10000
5000
0
*
*
CN% 100 75 50
SE% - 25 50
C
i) IE
Failure strain / %
20
15
10
5
0
N/S
N/S
***
CN% 100 75 50 25
IE% - 25 50 75
ii) SE
Failure strain / %
20
15
10
5
0
N/S
N/S
CN% 100 75 50
SE% - 25 50

Figure 5

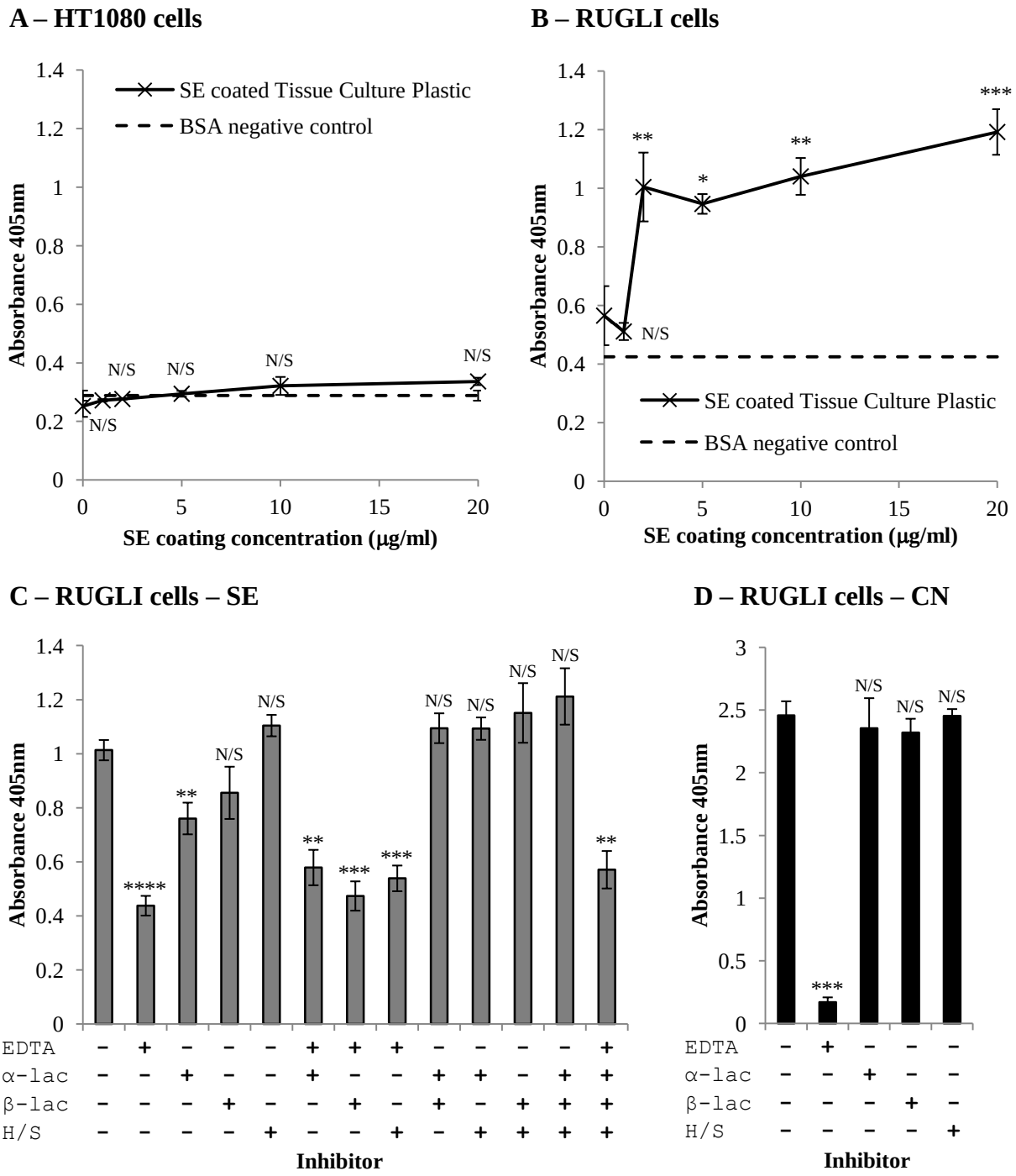
A – HT1080 cells
SE coated Tissue Culture Plastic
BSA negative control
Absorbance 405nm
SE coating concentration (µg/ml)
N/S
B – RUGLI cells
*
**
***
C – RUGLI cells – SE
D – RUGLI cells – CN
EDTA
α-lac
β-lac
H/S
Inhibitor

Figure 6

A – HT1080 cells

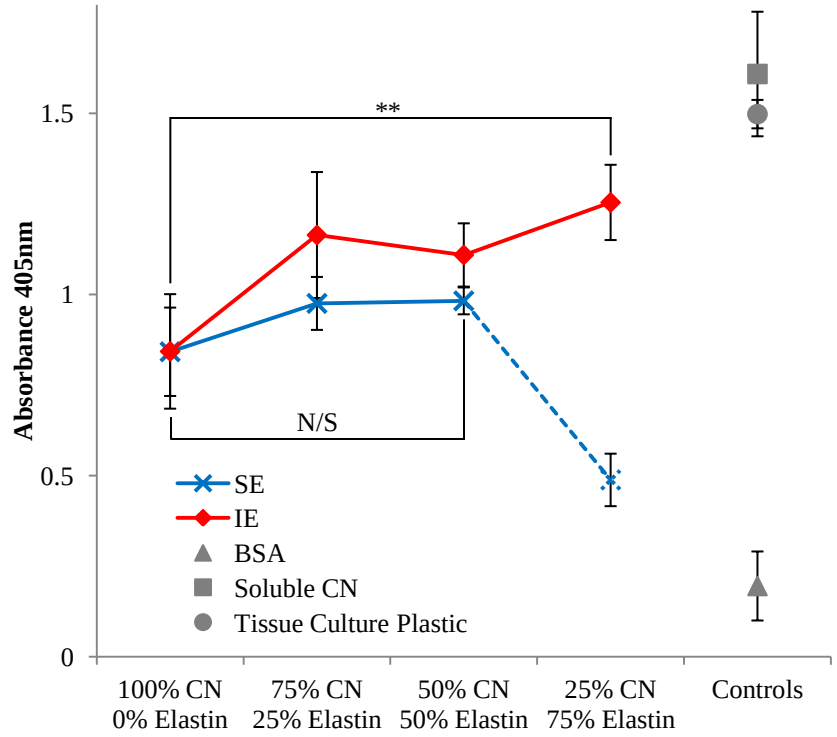

B – RUGLI cells

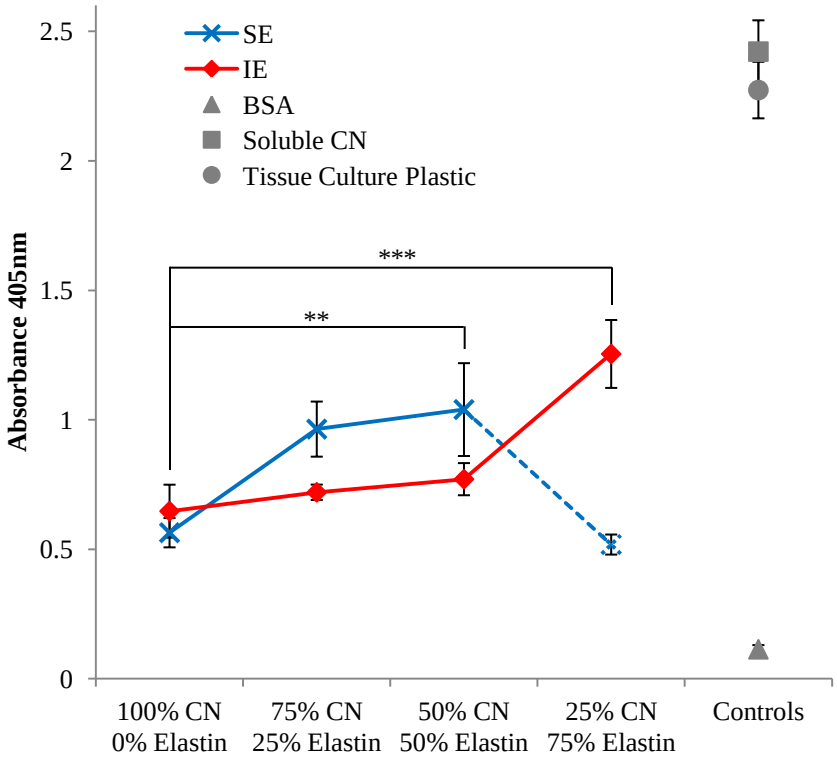

Figure 7

A – HT1080 cells

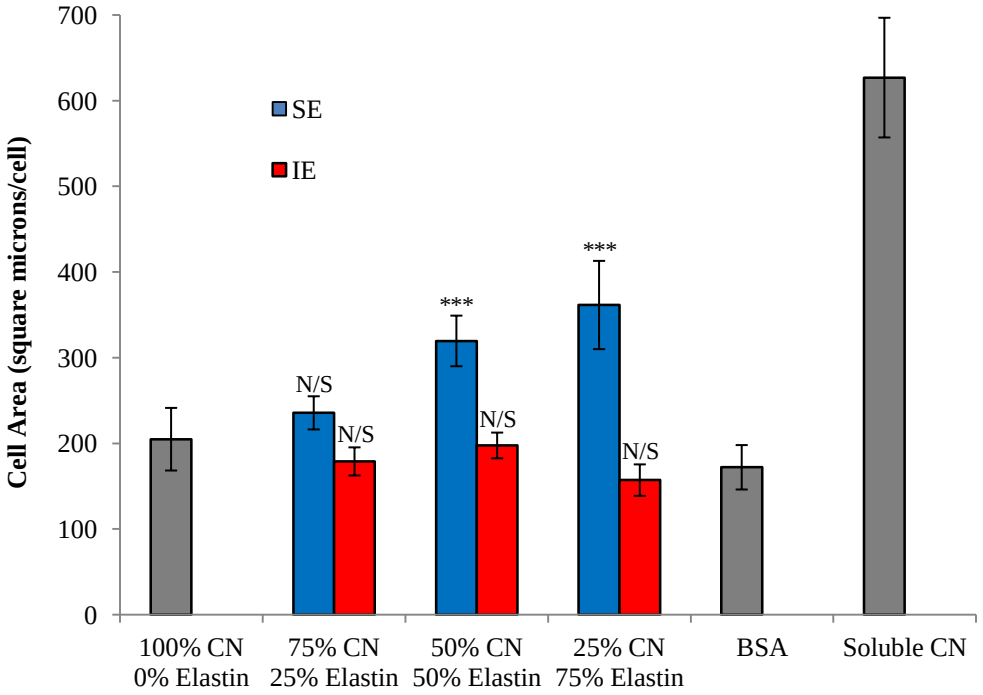

B – RUGLI cells

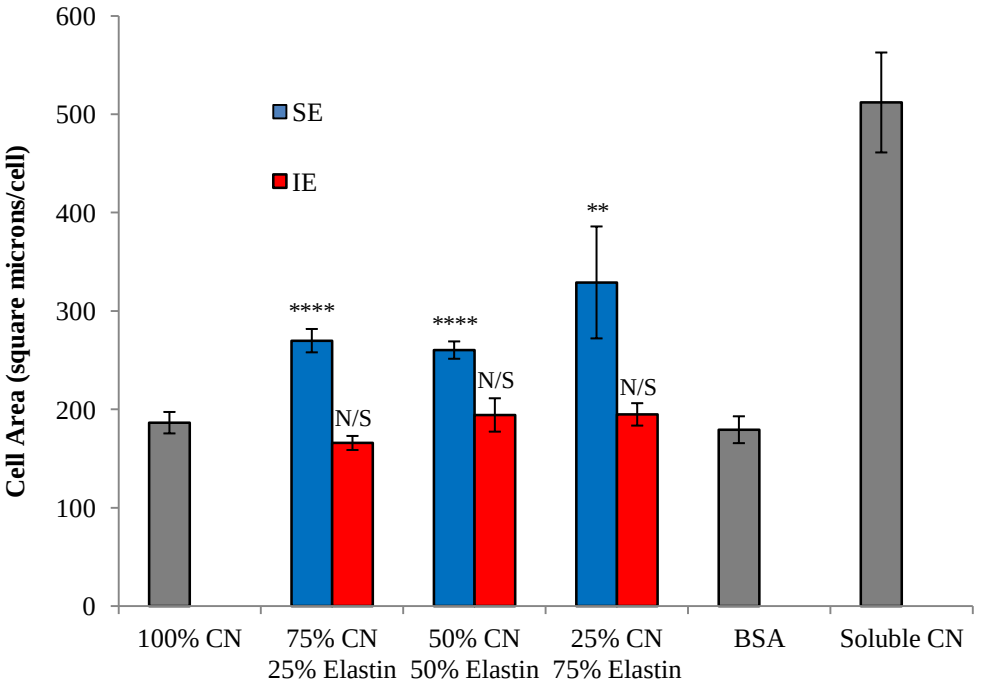

Figure 8

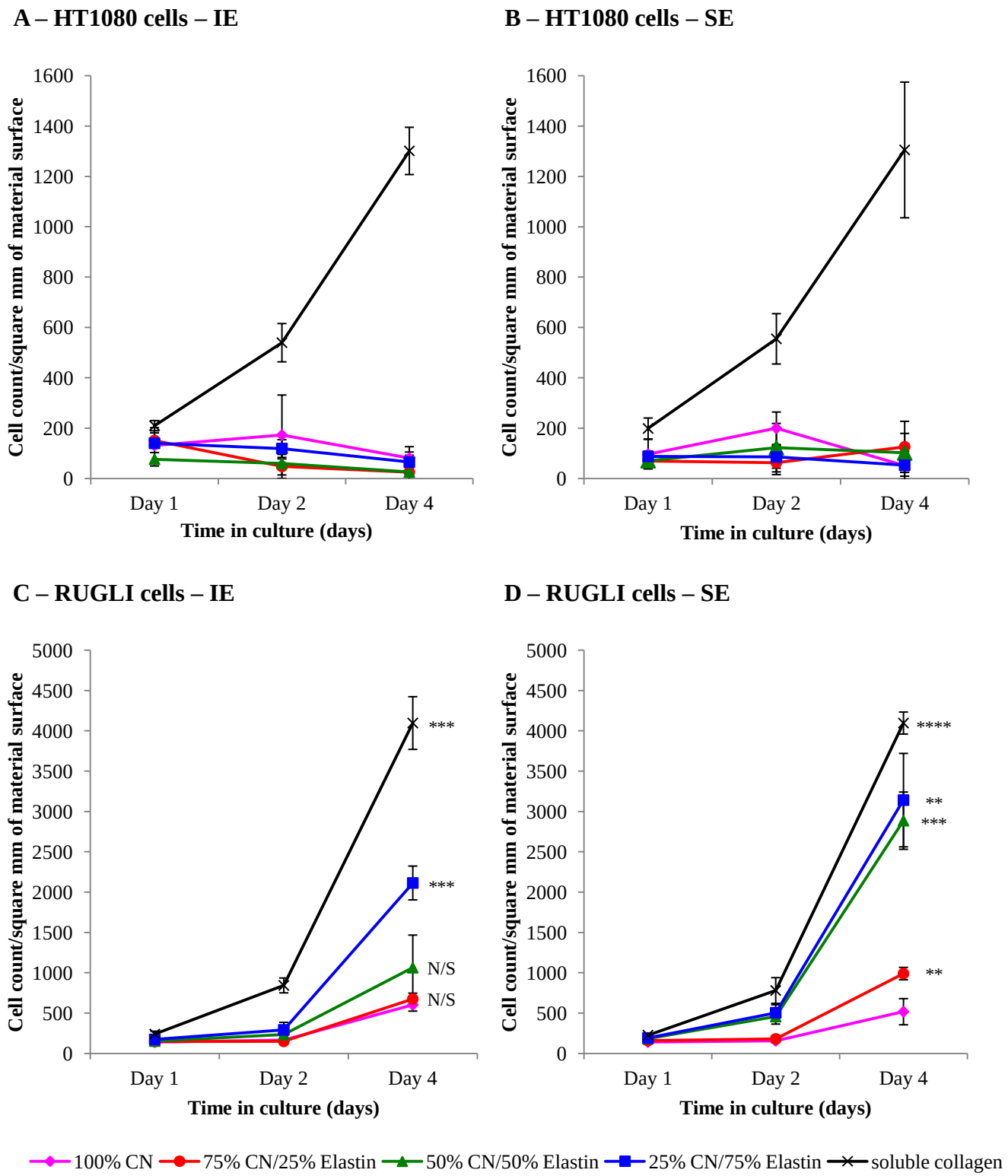
A – HT1080 cells – IE
B – HT1080 cells – SE
C – RUGLI cells – IE
D – RUGLI cells – SE
Cell count/square mm of material surface
Time in culture (days)
Day 1
Day 2
Day 4
0
200
400
600
800
1000
1200
1400
1600
500
1500
2000
2500
3000
3500
4000
4500
5000
***
N/S
****
**
100% CN
75% CN/25% Elastin
50% CN/50% Elastin
25% CN/75% Elastin
soluble collagen

Figure 9

A – RUGLI cell count at Day4 vs. IE content

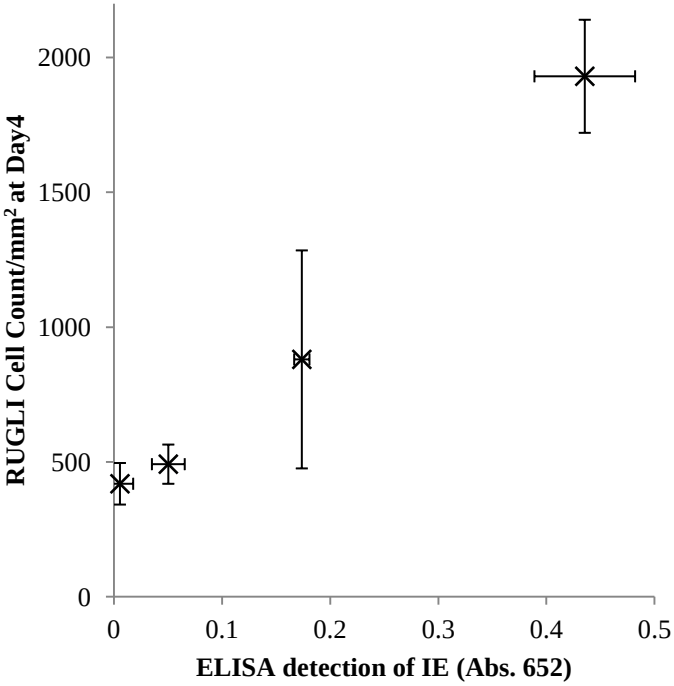

B – RUGLI adhesion vs. IE content

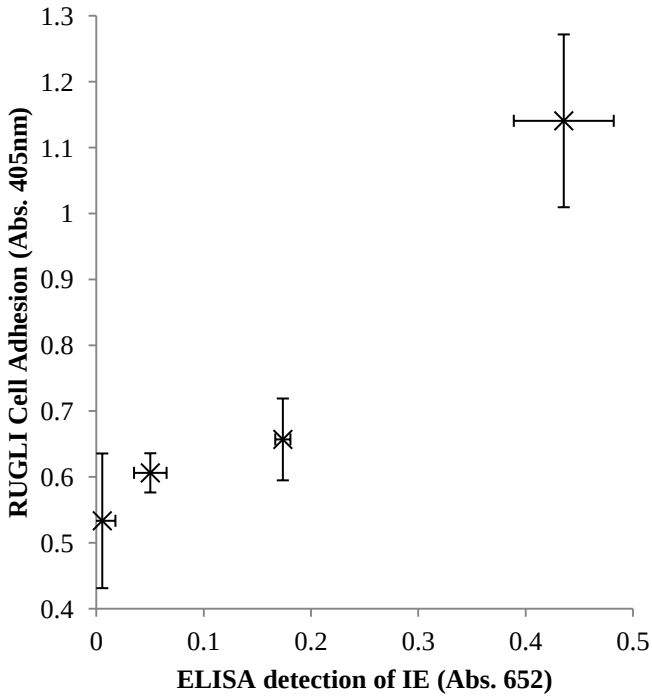

C – RUGLI cell count at Day4 vs. SE content

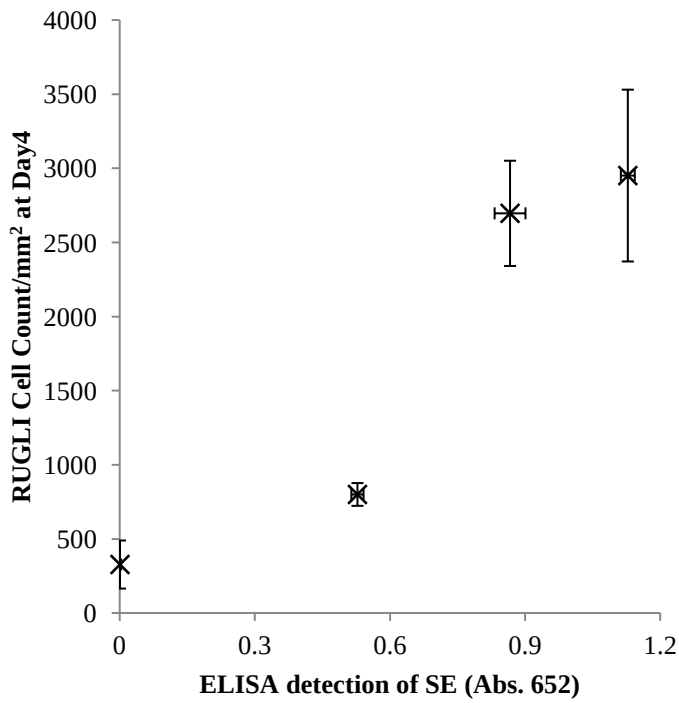

D – RUGLI adhesion vs. SE content

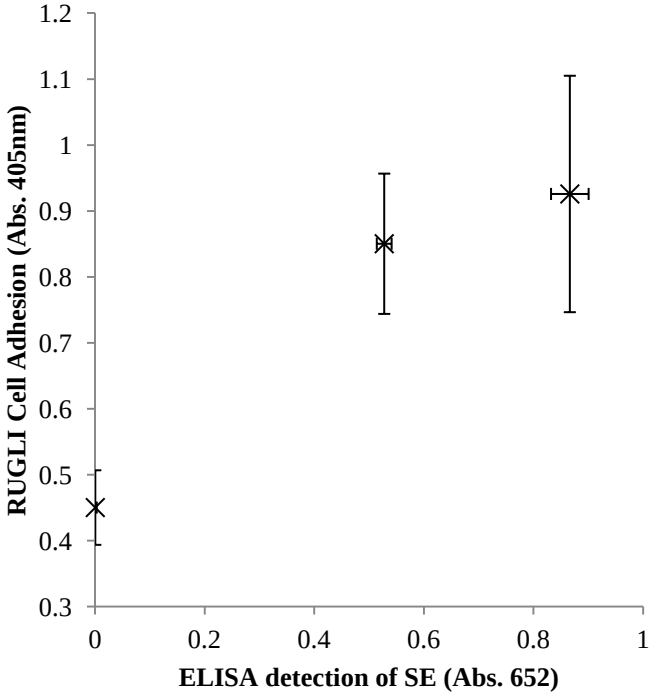

Supplementary figure 1

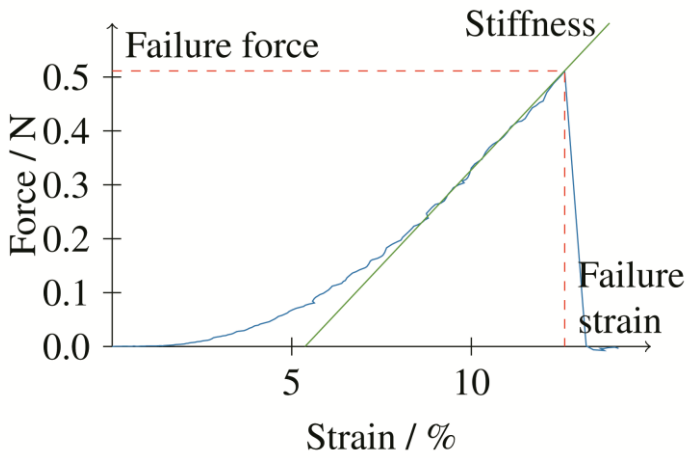

Supplementary figure 2A

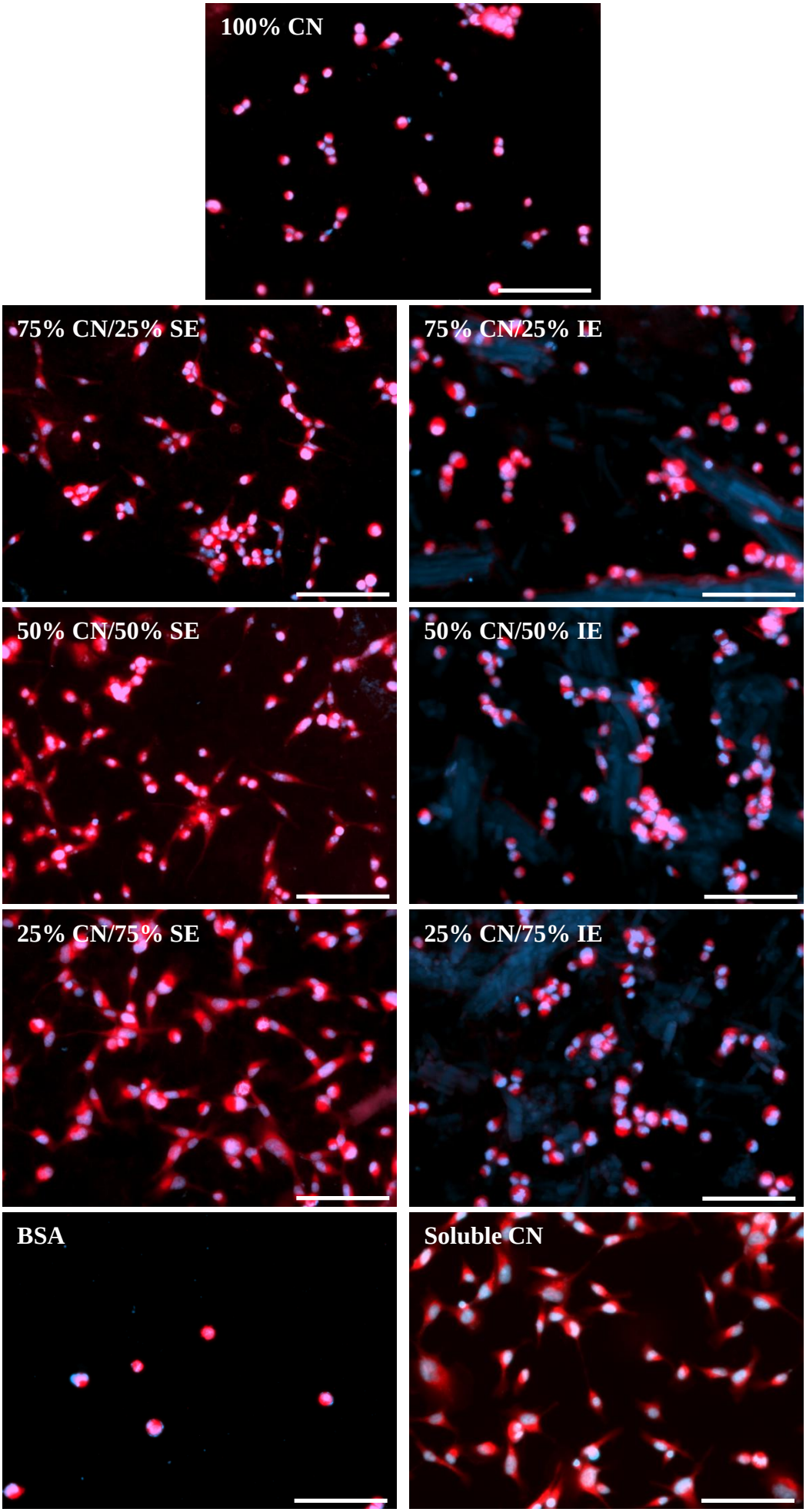

Supplementary figure 2B

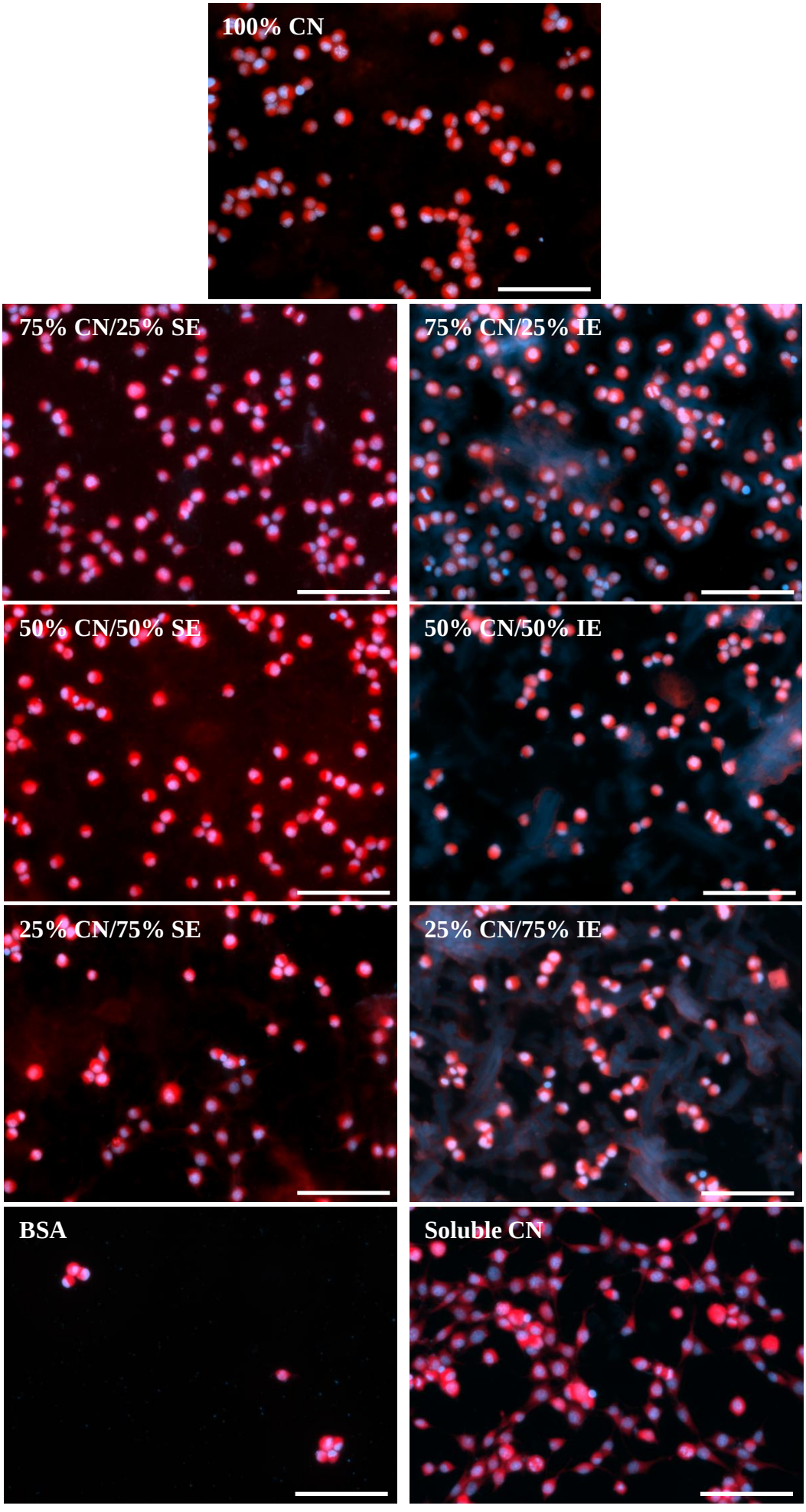

Supplementary figure 3